Intense Ultraviolet-Blue Photoluminescence from SiO₂ Embedded Ge Nanocrystals Prepared by Different Techniques

P. K. Giri[1, *], S. Bhattacharyya[1], R. Kesavamoorthy[2],
B. K. Panigrahi[2], and K. G. M. Nair[2]

[1] *Department of Physics, Indian Institute of Technology, Guwahati 781039, India*
[2] *Materais Science Division, Indira Gandhi Centre for Atomic Research, Kalpakkam 603102, India*

We have made systematic studies on the ultraviolet-blue photoluminescence (PL) from Ge nanocrystals (NCs) grown embedded in SiO₂ matrix. Embedded Ge NCs are grown by two different methods, namely, radio-frequency magnetron sputtering (SPT) and ion implantation (IMP). For comparison, Ar implanted SiO₂ layer was processed similarly and studied to isolate the contribution of Ge atoms in the observed PL. X-ray diffraction, optical Raman and low frequency Raman scattering studies confirm the presence of Ge NCs in samples prepared by SPT and IMP methods and Si nanoclusters in Ar implanted sample. Room temperature PL studies with 325 nm excitation show very strong UV-blue emission bands in the range 342–420 nm, and PL studies with 246 nm excitation show two strong UV emission bands at ∼285 nm and ∼393 nm in implanted samples. Deconvolution of UV-blue bands show that most of the emission peaks are not unique to the presence of Ge in the samples. Time resolved PL studies in the blue wavelength region show a fast decay dynamics (time constant of ∼1.0 ns), irrespective of the NC size. PL excitation spectroscopy measurements show a large Stoke's shift for the UV emission bands. Our results indicate that contrary to the literature reports, the ∼400 nm PL emission is band is not unique to the presence of Ge in the SiO₂ matrix and it is likely to originate from a defective NC/SiO₂ interface, irrespective of the species of NCs. Origin of various UV emission bands is discussed in the light of the experimental findings and literature reports.

Keywords: Ge Nanocrystal, UV Photoluminescence, Defects, Raman, PLE.

1. INTRODUCTION

In recent years, there is an upsurge of interest to understand the optical properties of Ge nanocrystals (NCs) in the quantum confinement regime, since these NCs appear to have promising light emitting and charge storage characteristics. Several studies on the optical properties of Ge nanocrystals (NCs) embedded in Si oxide films and on their photoluminescence (PL) mechanism have been reported.[1–3] Recently, violet-blue and blue PL emission have been reported from Ge implanted SiO₂ layers and there exist controversy regarding the origin of the violet-blue PL emission.[4, 5] Rebohle et al.[6] reported a strong blue-violet PL and electroluminescence from Ge-implanted and Si-implanted SiO₂ layer and they attributed the observed PL to neutral oxygen vacancies in SiO₂. Similarly, Sahoo

et al. observed stable violet emission from Ge implanted α-quartz and attributed it to Ge-related defects.[7] Zacharias and Fauchet[3] argued that ∼400 nm blue luminescence must be related to the formation of Ge or GeO₂ nanocrystals in the oxide matrix and they suggested that defects at the NC/matrix interface is responsible for the emission. On the other hand, Liao et al.[8] and Feinardi and Paleari[9] observed violet PL in SiO₂ samples that does not contain Ge atoms and the violet emission was attributed to oxygen deficient defects in SiO₂. Violet luminescence in Ge nanocrystals/Ge oxide structures formed by dry oxidation of polycrystalline SiGe has been attributed to defects at the NC Ge/GeO₂ interface.[10] Although the UV-violet and blue emissions have been reported from Si and Ge ion-implanted SiO₂ layers,[6, 11] no systematic studies have reported on the ultraviolet (UV) and violet PL emission from sputter deposited Ge NC.[3] It may be noted that strong ultraviolet PL from silicon oxide films prepared by

*Author to whom correspondence should be addressed.

magnetron sputtering has been reported.[12] Yang et al.[13] attributed it to interface defect, while Du et al.[14] attributed it to quantum confinement effect of Si NCs.

In this work, we report on the intense UV-blue photoluminescence from SiO₂ embedded Ge NCs prepared by sputter deposition and ion implantation methods. To understand the role of Ge atoms in the photoluminescence, we also study Ar implanted SiO₂ layer that was processed similar to the Ge implanted samples. Different samples are characterized by X-ray diffraction (XRD), optical Raman, low frequency Raman scattering (LFRS), steady-state and time-resolved photoluminescence (PL) and PL excitation spectroscopy (PLE) techniques. The steady state PL measurements are carried out using two different excitation sources: 246 nm, 325 nm. Possible origin of the UV-blue emissions at room temperature is explored by careful analysis of samples prepared with and without Ge content in the SiO₂ matrix.

2. EXPERIMENTAL DETAILS

We study primarily two sets of samples: one set prepared by radio-frequency (RF) sputter deposition method (SPT), and another set prepared by ion implantation method (IMP). In the SPT method, the Ge–SiO₂ thin films were deposited on (100) oriented *p*-type Si substrates by RF magnetron sputtering. The target used was a 2-inch Si wafer masked with Ge wafer pieces. The target to substrate distance was kept fixed at 6 cm and the working pressure was maintained at 0.11 Torr by introducing oxygen and argon in the ratio of 2:1. The depositions were carried out at a RF power 50 W for 1 hour. As-deposited samples are subsequently annealed at 700 °C (SPT1) and 900 °C (SPT2) for 1 hour in nitrogen ambient to grow embedded Ge NCs of various sizes.

In the IMP method, 300 keV Ge⁺ ions were implanted at room temperature on thermally grown (wet-oxidation) SiO₂ films of thickness ∼300 nm on Si(100) substrate with fluences 4×10^{16} (IMP1) and 1×10^{17} (IMP2) ions/cm². Another sample was prepared by implanting 100 keV Ar⁺ ions into SiO₂ layer (thermally grown) at a dose of 5×10^{16} cm⁻² (Ar1). All the implanted SiO₂ layers were annealed at 1000 °C for 1 hour in argon gas ambient. Details of the samples with nomenclature are presented in Table I.

Table I. Details of the samples studied in the present work.

Preparation method	Deposition time/ion dose (cm⁻²)	Annealing temperature (°C)	Sample name	Average size of Ge NCs (nm)
RF sputtering	1 hr	700	SPT1	7
RF sputtering	1 hr	900	SPT2	9
Ge⁺ implanted SiO₂	4×10^{16}	1000	IMP1	9
Ge⁺ implanted SiO₂	1×10^{17}	1000	IMP2	13
Ar⁺ implanted SiO₂	5×10^{16}	1000	Ar1	—

XRD measurements were performed in grazing incidence mode using a powder diffractometer (Seifert 3003 T/T) in thin film mode. Raman spectra for all the samples were recorded in the backscattering geometry using vertically polarized 488 nm Argon–ion laser beam, double grating monochromator and cooled photomultiplier tube. LFRS spectra were recorded from 5 to 40 cm⁻¹ at steps of 0.5 cm⁻¹ using the same set up. Steady state PL measurements were made using a 325 nm He-Cd laser along with a Jobin-Yvon T64000 spectrometer equipped with a cooled charged coupled detector. The PL decay measurements were performed using 378 nm excitation pulse of 1.32 ns duration using a commercial fluorescence lifetime setup with a time resolution of 0.113 ns (Model IBH Fluorocube). In the PL decay measurement, a cutoff filter was placed before the emission detector to block the light below the wavelength 385 nm. PL decay measurement was also carried out at fixed wavelength (400 nm) using a picosecond time resolved spectrometer. PL excitation spectra and deep UV emission spectra (with 246 nm excitation) were recorded using a commercial fluorimeter (Thermo Electron, AB2) with a monochromated Xenon lamp source.

3. RESULTS AND DISCUSSION

3.1. XRD and Raman Scattering

Figures 1(a and b) shows XRD pattern for the samples prepared by IMP and SPT methods. Both the samples show Ge(111) and Ge(311) peaks at 27.3° and 45.3°, and these peaks are the evidences for Ge NCs present in these samples. The IMP samples show additional peak for SiO₂(100) and SPT1 sample show peak for GeO₂(101) in addition to the Ge NC peaks. Figure 1(c) shows the typical Raman spectra for IMP2 and SPT2 showing distinct peak at ∼300 cm⁻¹ indicating the presence of Ge nanocrystals. Raman bands at ∼420 cm⁻¹ and 520 cm⁻¹ corresponds to scattering from optical phonons involving localized Si–Si motion in the neighborhood of one or more Ge atoms in the SiO₂ matrix, and Si–Si vibration modes, respectively.[15] Effect of strain and phonon confinement is apparent in the broad Raman line shape of the ∼300 cm⁻¹ peak. The relatively broad line width is due to size distribution as well as phonon confinement effect. In SPT2, the phonon confinement effect is overshadowed by the strain effect which causes slight upshift of Raman peak thus compensating for the downshift expected from confinement effect.[16]

Sizes of the small NCs are estimated from the LFRS studies. LFRS is a powerful technique to study the confined acoustic phonon modes in NCs and to find the crystallite size from the measurement of low frequency phonon modes. LFRS peak frequencies are inversely proportional to the size of the NCs.[17] Figure 2 shows the characteristic LFRS spectra from SPT2, IMP1 and Ar1 showing distinct peak features at very low frequency due to presence of
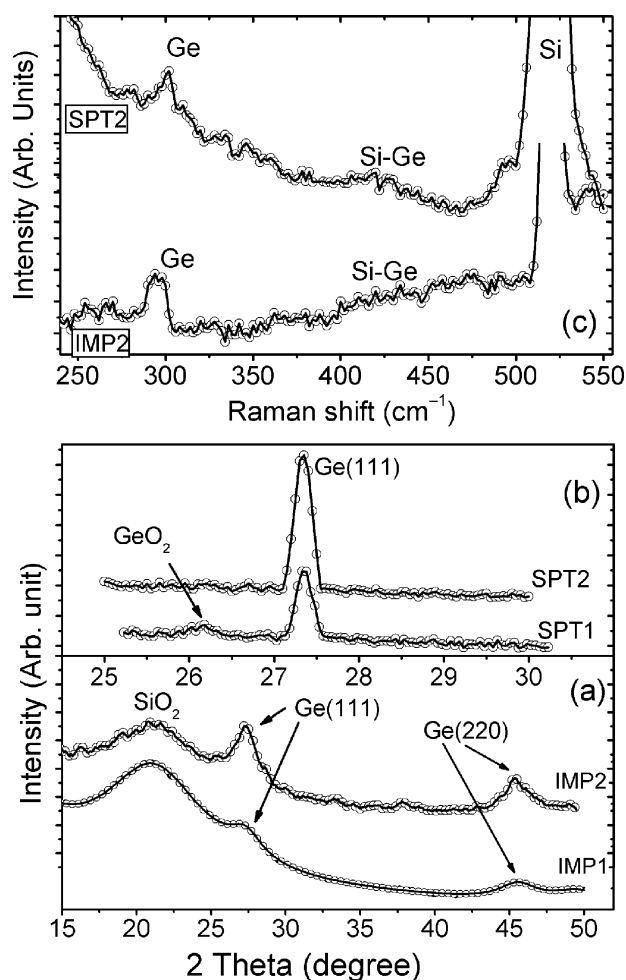
Fig. 1. (a) XRD pattern for IMP1 and IMP2, (b) SPT1 and SPT2 samples showing Ge(111) and Ge(311) NCs. (c) Optical Raman spectra for IMP2 and SPT2 showing Ge–Ge, Si–Ge and Si–Si phonon modes at ~300 cm^{-1}, ~420 cm^{-1} and 520 cm^{-1}, respectively.

NCs or nanoclusters. Since the LFRS peaks are very close to the Rayleigh tail, actual peak position is extracted from fitting Lorentzian line shape to the experimental data. In SPT2 and IMP1, the peaks are definite signature of surface acoustic phonon modes of Ge NCs, while in Ar1 the low frequency peak can be attributed to Si nanoclusters that form after Ar ion implantation followed by annealing. The mechanism of forming Si nanoclusters in Ar implanted SiO_2 may be as follows: during implantation the energetic Ar ions causes displacement of Si atoms in the Si-rich oxide (SiO_x), which can aggregates and form nanoclusters or nanocrystals of Si during thermal annealing. We have recently shown formation of Si nanolcuster in Ge implanted SiO_2 layer.[18] Thus, the presence of Si nanocluster/NCs in Ar implanted sample is confirmed from Figure 3(c). From the measured low frequency modes the NCs sizes can be calculated using the standard formula for spheroidal mode in Ge NCs:[17] $\nu_0^S = 0.7 v_t/dc$ $(n = 0)$, where c is the velocity of light, d is the average diameter of the NCs, and v_t is the transverse velocity of sound in
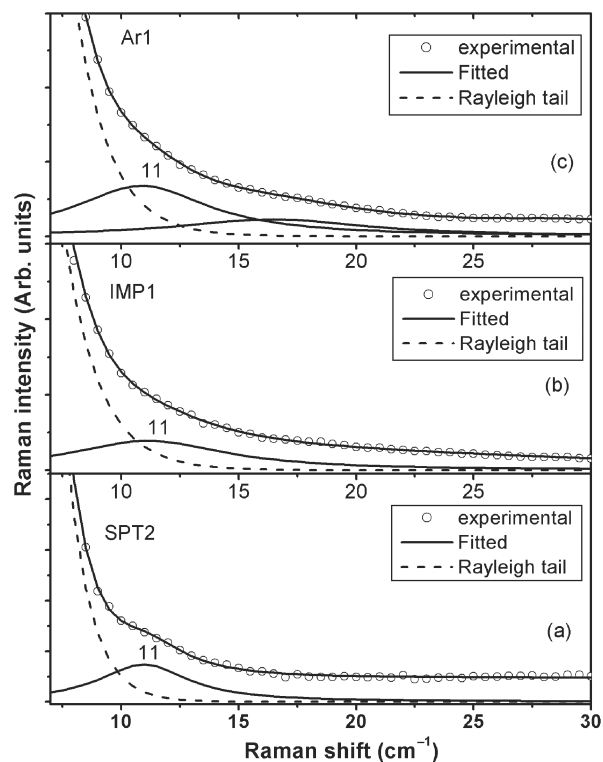
Fig. 2. Typical LFRS spectra for (a) SPT2 and (b) IMP1 samples showing surface acoustic phonon modes of Ge NCs. (c) LFRS spectra of Ar1 showing acoustic phonon modes indicating formation of Si NCs/nanoclusters embedded in SiO_2 matrix. Symbols are experimental data and solid lines are the fits with Lorentzian line shape and dashed line is the Rayleigh tail.

Ge NCs. We have assumed a $v_t = 3.25 \times 10^5$ cm/s for Ge. Neglecting the strain and shape effect on the mode frequency, the NC sizes are calculated and shown in Table I. In SPT2, high resolution TEM imaging shows Ge NCs of size ~7 nm,[16] which is comparable to the size of ~9 nm as estimated from LFRS study.

3.2. Steady State Photoluminescence

Previously, our room temperature PL studies with 488 nm excitation showed broad visible peak centered at ~540 nm (2.30 eV) for IMP as well as SPT samples, irrespective of NC size and NC species[16] and it was attributed to oxygen deficient defects in SiO_2 matrix. Here, we focus on the UV excitation source and UV-blue emission bands for various samples. It is worth mentioning that Fourier transform infrared spectroscopy and Rutherford back scattering analysis in both the samples show highly oxygen deficient oxide matrix (SiO_x, $x < 2$) and nature of the oxides is different in differently prepared samples. Thus, oxygen deficient defects in SiO_2 are expected to play a significant role in the PL emission. Note that thermally grown oxide quality is superior to the oxide quality grown by sputter deposition method. However, subsequent implantation of thermal oxide causes breaking of bonds and oxygen deficient defects in SiO_2 matrix.
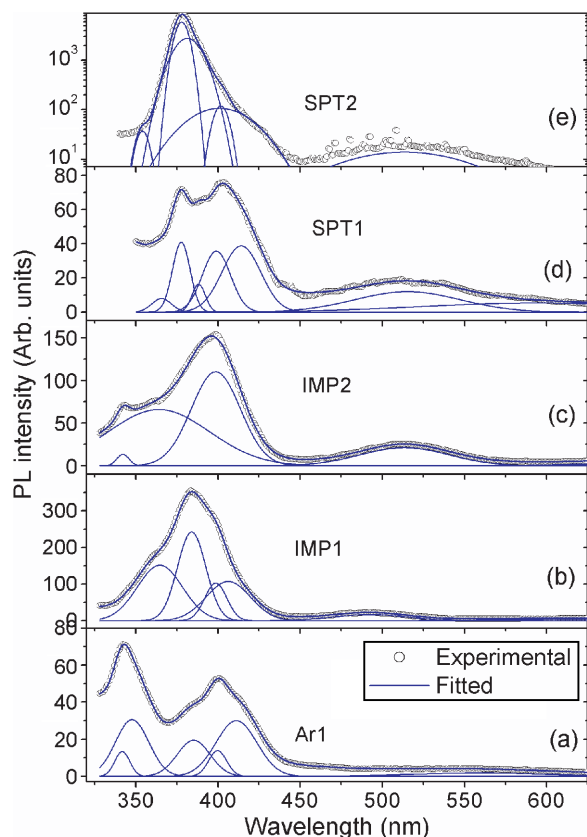
Fig. 3. PL spectra obtained with 325 nm excitation for (a) Ar1, (b) IMP1, (c) IMP2, (d) SPT1, and (e) SPT2. Multiple peaks are fitted with Gaussian line shape for the emission bands in the UV and visible region. Peak positions extracted from fitting are given in Table II. Some of the UV and visible region peaks are common to all samples. Note that owing to high intensity of UV emission in SPT2, *Y*-axis in Figure 4(e) is plotted in logarithmic scale.

First, we study the PL emission with 325 nm excitation from all five samples (Ar1, IMP1, IMP2, SPT1, and SPT2). Figure 3 shows several strong emission bands in the UV-blue region in addition to the broad PL band near ∼500 nm. The actual peak positions are obtained by deconvolution of the experimental spectra assuming Gaussian line shape for the PL emission bands. The fitted peaks for different samples are shown as solid lines and experimental data are shown with symbols. The summary of the fitted peaks are presented in Table II. Note

Table II. Summary of the deconvoluted peaks for the PL spectra obtained with different excitation wavelengths (λ_{exc}).

Samples	Centre of the PL peaks (nm)							
	$\lambda_{exc} = 325$ nm							$\lambda_{exc} = 246$ nm
Ar1	342, 348	—	385	400, 411	—	559	285	—
IMP1	—	364	384	398, 406	492	634	285	393
IMP2	342	364	—	398	513	686	285	393
SPT1	—	366	378, 388	399, 414	515	594	—	—
SPT2	354	—	378, 382	401	514	593	—	—

that strong UV bands at ∼342 nm, 378–385 nm and blue band at ∼400 nm are common to all samples including Ar1, where Ge atoms are not present. Hence, these bands are not necessarily related to Ge-related emitting centers, contrary to the belief that ∼400 nm band is related to Ge related centers. Thus these emission bands must be attributed to defects in the SiO$_x$ matrix or defects at the interface between NC and SiO$_x$. Since these bands are not found prior to annealing, purely matrix defects are not involved for the emission. Note that all three samples have a NC/SiO₂ interface in common, although the nature of the oxide is different in different samples due to different preparation conditions.

Further PL studies were performed with varying excitation wavelength using a Xenon lamp source with monochromator. Figure 4(a–c) shows the PL emission spectra with 246 nm excitation source for IMP samples and Figure 4(d) shows the spectra for a unimplanted SiO₂ layer that was heat treated under identical condition. While the deep UV emission bands at ∼285 nm is common to all three implanted samples including Ar1, the ∼393 nm band intensity is relatively low in IMP2 sample and negligibly low for Ar1. Note that SPT samples do not exhibit any measurable intensity of UV emission under 246 nm excitation. Therefore, the ∼285 nm band is not specific to Ge atoms in the SiO₂ matrix (See Table II). It is likely to be related to defects in the SiO$_x$ matrix created by ion implantation. Note that unimplanted SiO₂ do not show any
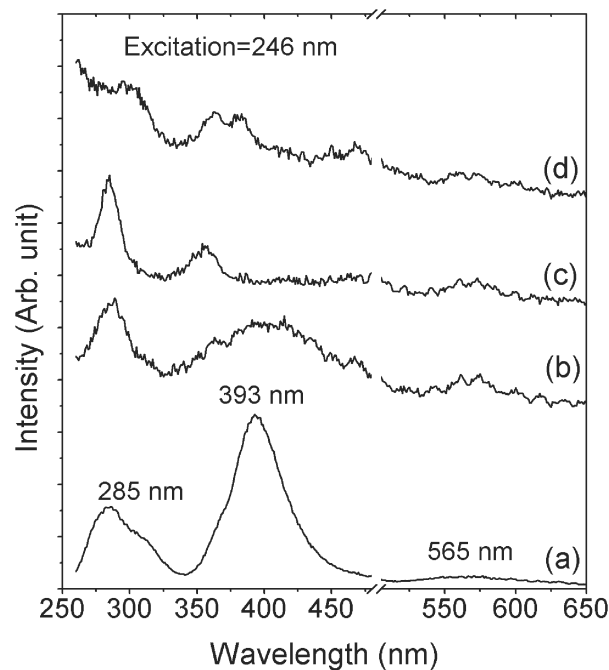
Fig. 4. PL spectra recorded with 246 nm excitation for: (a) IMP1, (b) IMP2, (c) Ar1 and (d) unimplanted SiO₂ film (annealed). Three major emission bands are marked with respective peak positions in nm unit. The ∼285 nm band is common to all implanted SiO₂ layer. *X*-axis is shown with a break in the region 480–505 nm to omit the band due to 2nd harmonics of the incident wavelength.

significant UV emission as compared to the IMP samples. It may be noted that PLE measurements in IMP1 and IMP2 showed distinct excitation peak at ~246 nm for emission at ~390 nm and thus we studied the PL emission spectra for 246 nm excitation and found additional UV bands.

3.3. PL Excitation Spectroscopy

In order to understand better the nature of the defects involved in the UV emission band obtained with 325 nm excitation, we perform PL excitation spectroscopy (PLE) by keeping the emission wavelength fixed at 378 nm for SPT1 and SPT2 and at 348 nm for Ar1. Figure 5 shows the PLE spectra that show a broad excitation peak centered at ~320 nm for the 378 nm emission from both SPT1 and SPT2 samples. Ar1 shows a similar excitation band at ~318 nm for the emission at ~350 nm. Thus, the samples exhibit very large Stokes shift (~0.5 eV) between the absorption and emission of a specific band. The Stokes shift characterizes the energy relaxation between the excitons that takes place within inhomogeneously broadened absorption line and inhomogeneous broadening may result from interfacial roughness, defects, impurities and other structural imperfection.[19] In the present case besides the matrix defects, interfacial roughness is likely to be present due to the formation of NCs in the defective oxide matrix. Hence, the observed Stoke's shift is a possible indicator of a defective interface between NC and SiO_2 matrix in all

three samples, and the UV emission bands may be related to the interface defects.

3.4. Time Resolved PL Studies

Figures 6(a and b) shows the PL decay dynamics for the SPT1 and SPT2 samples excited with 378 nm excitation pulse. PL emission was monitored for all wavelengths above 385 nm in the visible range. Figure 6(c) shows the PL decay dynamics for SPT1 monitored at a fixed wavelength of 400 nm with the same excitation source. Reference data (system response) was subtracted from the sample data to fit the decay curves shown in Figure 6. The resulting decay curves show a double exponential dynamics of recombination with time constants $\tau_1 = 1.0$ ns and $\tau_2 = 5.2$ ns as obtained from fitting, for both the samples. As the time constants are independent
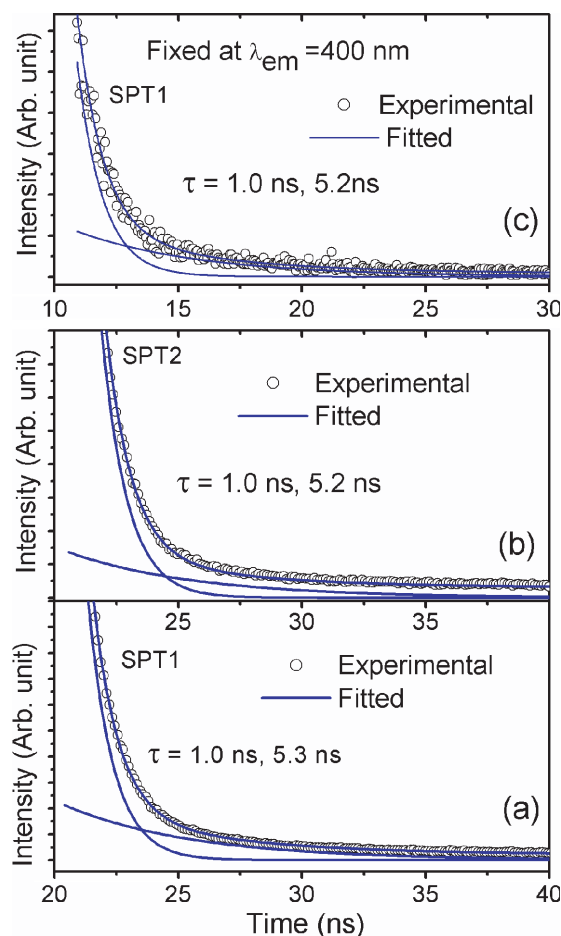
Fig. 6. Room temperature PL decay dynamics of blue-violet emission band (>385 nm) from (a) SPT1 and (b) SPT2 samples. (c) PL decay dynamics for SPT1 recorded at a fixed emission wavelength (400 nm). The experimental data is plotted after subtracting the reference data. The data (symbols) could be fitted (solid line) well with two exponentials with time constants (τ) 1.0 ns and 5.2 ns in both the samples, independent of the NC size. Note that the amplitude of decay component with 5.2 ns time constant is several orders of magnitude lower than the component with 1.0 ns time constant.

Fig. 5. PLE spectra for (a1) SPT1, (b1) SPT2, and (c1) AR1. For comparison, the respective emission spectrum is shown in the right hand side. The PL emission was monitored at a fixed wavelength as indicated for each curve.

of the size of the Ge NCs present in the samples, the fast decay dynamics is unlikely to originate from the recombination at the core of the NCs. From the fitting parameters, it is found that amplitude of τ_1 component of decay is 9 orders of magnitude higher that the amplitude of τ_2 component. The fast decay can be understood considering the effect of nonradiative recombination at the deep level defects using the Shockley-Read-Hall recombination theory. Thus τ_1 refers to nanradiative recombination at the defects, while τ_2 represents the radiative recombination at the defect sites in the SiO₂ matrix or at the NC/SiO₂ interface. Similar fast PL decay dynamics was observed for visible PL from Ge NCs prepared by ion-implantation.[20] A fast (∼4 ns) decay dynamics was observed for the UV PL from defects in porous silica.[21] Zacharias and Fauchet observed a nanosecond PL dynamics for the ∼400 nm band in sputter deposited Ge NCs and the fast response was attributed to defects at the nanocrystal/matrix interface.[3] We attribute the observed fast decay dynamics to the defects at the NC/SiO₂ interface.

3.5. Discussion

In the literature, ∼400 nm blue peak has been assigned to Ge/O related defects in sputter deposited Ge NCs[3] or the defects at the interface between Ge NC and SiO₂ matrix.[22] However, our results indicate that ∼400 nm emission is not unique to the presence of Ge in the SiO₂, since it is found in Ge free SiO₂ sample as well. Note that ∼400 nm band is very intense in both SPT1 and Ar1 as compared to a lower intensity peak in SPT2. The ∼393 nm band with 246 nm excitation is also strong in IMP1. It is also noteworthy that locations of the emission bands are dependent on the excitation wavelength, indicating a broad density of states present in the band structure of the host matrix and a section of it takes part in the optical transitions monitored with a particular excitation wavelength. There are two possible sources for the blue emission bands. Firstly, since oxygen deficient defects are common to all samples and density of these defects reduces with higher annealing temperature/time, some form of oxygen deficient defects in SiO₂ is most likely candidate for these strong emission bands. Secondly, the interface between NCs and surrounding defective matrix changes as a function of annealing temperature/time. A NC/SiO₂ interface is common to all five samples including Ar1, where Si NCs are present as revealed from LFRS studies. Thus, it is the interface between the nanocluster/SiO₂ matrix that may be responsible for these bands, irrespective of the species of nanocluster. In SPT2 sample, oxide quality is expected to be improved due to higher temperature of annealing and we observe very low intensity of the ∼400 nm peak. The NC/SiO₂ interface is different in various samples (obtained with different processing conditions) and it gives rise to variations in the UV emission bands (343, 364 nm,

377 nm), as observed in Figure 5. Note that the band gap of nonstoichiometric SiO$_x$ ranges from 1.8 to 4.0 eV and depends strongly on its composition.[3] Observation of a lower wavelength (354 nm) PL peak in SPT2 compared to SPT1 sample (366 nm) is consistent with the fact that bandgap of SiO$_x$ is higher in SPT2 due to higher temperature of annealing. In case of Ar1, the oxide matrix is highly defective as revealed from FTIR analysis (not shown) and hence a lower wavelength emission may be expected. Note that the UV emission band at ∼285 nm is also not specific to presence of Ge atoms in the SiO₂ matrix. Similar UV emission has been previously reported for Ge implanted SiO₂ film[4] and unirradiated SiO₂ film containing different impurities.[9] Oxygen deficient defects in SiO₂ with different environment are believed to result in different UV bands.[9]

Tong et al. observed adjustable UV emission bands from silicon rich oxide films.[23] Kim et al.[24] observed an UV PL band at 365 nm from silicon rich oxide layer and ascribed it to the hole trapped E' center. However, E' center was found to anneal out completely in the temperature range 500–700 °C.[12] Hence, any mechanism related bulk defects in SiO₂ seem unreasonable for the 342–378 nm bands. In sputter deposited silicon oxide, Song et al.[12] argued that a two fold coordinated Si defect of SiO₂ (O–Si•ₓ–O) at the interface between NC Si and the SiO₂ is responsible for the 370 nm PL band. We believe that as the interface quality improves with higher annealing temperature, the 377 nm band slowly disappears and the 361 nm band appears stronger as a result of higher density of Ge NCs forming the interface states. Thus, the UV bands are likely to result from recombination at defects at the NC/SiO₂ interface. This proposition for the UV band is supported by the PLE data, which show a large Stokes shift. However, more studies are required to pinpoint the exact source of UV emissions.

4. CONCLUSIONS

We report on the intense UV-blue PL emission from SiO₂ film containing Ge NCs prepared by two independent methods. Sources of various PL bands are studied by steady state PL, time resolved PL and PL excitation spectroscopy. The fast decay dynamics (∼1 ns) of the blue PL band indicates the involvement of defects for the emission. A large stokes shift (∼0.5 eV) for the UV emission bands indicate the possible involvement of interface defects for the observed UV bands. The UV bands at ∼285 nm, ∼342 nm and ∼379 nm and the blue emission band at ∼400 nm is found to be independent of presence of Ge atoms in the matrix, and is sensitive to the nature of environment the defect experiences due to different surroundings. Oxygen deficient defects in SiO₂ matrix with different defect/impurity environment is believed to give rise to various UV emission bands. It is likely that

a two-fold coordinated Si defect at the NC/SiO_2 interface may be responsible for the ~400 nm blue PL.

References and Notes

1. K. S. Min, K. V. Shcheglov, C. M. Yang, M. A. Atwater, M. L. Brongersma, and A. Polman, *Appl. Phys. Lett.* 68, 2511 (**1996**).
2. X. L. Wu, T. Gao, G. G. Siu, S. Tong, and X. M. Bao, *Appl. Phys. Lett.* 74, 2420 (**1999**).
3. M. Zacharias and P. M. Fauchet, *Appl. Phys. Lett.* 71, 380 (**1997**).
4. J. Y. Zhang, Y. H. Ye, X. L. Tan, and X. M. Bao, *J. Appl. Phys.* 86, 6139 (**1999**).
5. S. H. Choi, S. C. Han, and S. Hwang, *Thin Solid Films* 413, 177 (**2002**).
6. L. Rebohle, J. von Borany, R. A. Yankov, W. Skorupa, I. E. Tyschenko, H. Fröb, and K. Leo, *Appl. Phys. Lett.* 71, 2809 (**1997**).
7. P. K. Sahoo, S. Dhar, S. Gasiorek, and K. P. Lieb, *J. Appl. Phys.* 96, 1392 (**2004**).
8. L. S. Liao, X. M. Bao, X. Q. Zheng, N. S. Li, and N. B. Min, *Appl. Phys. Lett.* 68, 850 (**1996**).
9. F. Meinardi and A. Paleari, *Phys. Rev. B* 58, 3511 (**1998**).
10. M. Avella, A. C. Prieto, J. Jimenez, A. Rodriguez, J. Sangrador, and T. Rodriguez, *Solid State Comm.* 136, 224 (**2005**).
11. R. Salh, L. Fitting, E. V. Kolesnikova, A. A. Sitnikova, M. V. Zamoryanskaya, B. Schmidt, and H.-J. Fitting, *Semiconductor* 41, 381 (**2007**).
12. H. Z. Song, X. M. Bao, N. S. Li, and X. L. Wu, *Appl. Phys. Lett.* 72, 356 (**1998**).
13. X. Yang, X. L. Wu, S. H. Li, H. Li, T. Qui, Y. M. Yang, P. K. Chu, and G. G. Siu, *Appl. Phys. Lett.* 86, 201906 (**2005**).
14. X. W. Du, L. Y. Liu, P. Yao, and L. Cui, *J. Appl. Phys.* 100, 076102 (**2006**).
15. M. I. Alosno and K. Winer, *Phys. Rev. B* 39, 10056 (**1989**).
16. P. K. Giri, S. Bhattacharyya, K. Das, S. K. Roy, R. Kesavamoorthy, B. K. Panigrahi, and K. G. M. Nair, *Semicond. Sci. Technol.* 22, 1332 (**2007**).
17. E. Duval, A. Boukenter, and B. Champagnon, *Phys. Rev. Lett.* 56, 2052 (**1986**).
18. P. K. Giri, R. Kesavamoorthy, S. Bhattacharya, B. K. Panigrahi, and K. G. M. Nair, *Mater. Sci. Engg. B* 128, 201 (**2006**).
19. G. D. Gilliland, *Mater. Sci. Engg. R* 18, 99 (**1997**).
20. P. K. Giri, R. Kesavamoorthy, B. K. Panigrahi, and K. G. M. Nair, *Solid State Commun.* 133, 229 (**2005**).
21. N. Chiodini, F. Meinardi, F. Morazzoni, A. Paleari, R. Scotti, and D. Di Martino, *Appl. Phys. Lett.* 76, 3209 (**2000**).
22. M. I. Ortiz, A. Rodríguez, J. Sangrador, T. Rodríguez, M. Avella, J. Jiménez, and C. Ballesteros, *Nanotechnology* 16, S197 (**2005**).
23. J. F. Tong, H. L. Hsiao, and H. L. Hwang, *Appl. Phys. Lett.* 74, 2316 (**1999**).
24. K. Kim, M. S. Suh, T. S. Kim, C. J. Youn, E. K. Suh, Y. J. Shin, K. B. Lee, H. J. Lee, M. H. An, H. J. Lee, and H. Ryu, *Appl. Phys. Lett.* 69, 3908 (**1996**).

RESEARCH ARTICLE